ICSV13 - Vienna
The Thirteenth International Congress on Sound and Vibration
Vienna, Austria, July 2-6, 2006

PHASE AND FREQUENCY SPECTROGRAMS

François Léonard

Institut de recherche d'Hydro-Québec
1800 boul. Lionel-Boulet, Varennes, Québec, Canada, J3X 1S1
leonard.francois@ireq.ca

Abstract

The short-time Fourier transform (STFT) yields a complex distribution function which includes amplitude and phase information. Until recently, the results of STFT calculations have always been presented in the form of a power spectrogram where only the amplitude value of the STFT is shown. However, the amplitude value contains only a small part of the phase information and reciprocally for the phase value, which means that we are deprived of an important source of information. The aim of this paper is to present two different ways of using the STFT phase information. The frequency spectrogram is calculated from the phase difference between each time slice of the STFT. The frequency spectrogram shows the drift on the instantaneous frequency of each spectral component. The time integral of the frequency spectrogram yields the phase spectrogram. The phase spectrogram supplies information about the phase modulations of each spectral component around a reference time point. These tools have proven to be useful complements to the power spectrogram. Digital simulations together with examples from measurements of mechanical vibrations bear witness to their usefulness and accuracy.

INTRODUCTION

D. Gabor [1] and J. Ville [2] introduced the concept of time-frequency representation in the mid 1940s. Since then, many efforts have been invested to combine and consolidate the different approaches under Cohen's class [3]. However, although certain algorithms make use of the phase in the time-frequency plane [4-6], no author has come up with a way to graphically represent the phase in this plane.

In the proposed algorithm, our starting point is the Short Time Fourier Transform (STFT)

$$F_s(\tau,\nu) = \int_{-\infty}^{\infty} s(t)\cdot h^*(t-\tau)e^{-j2\pi\nu t}dt \quad , \tag{1}$$

of a continuous analytical time signal s(t),with $F_S(\tau,\nu)$ denoting the complex distribution function and $h^*(t-\tau)$, the conjugate of the spectral window used as a time-frequency kernel. The resulting product $F_s(\tau,\nu)\cdot F_s^*(\tau,\nu)$ gives the spectrogram. In this text, we will refer to the 'power spectrogram' when we refer to this product, as opposed to the 'phase spectrogram' and 'frequency spectrogram', which will be introduced later.

For real measurements, the computer processes a discrete real signal s_n and the STFT becomes

$$S_{m,i} = \sum_{n=0}^{N-1} s_{n+m\cdot l}\cdot h_n \cdot e^{-j2\pi\frac{i}{N}n} \quad , \; i \in \{0,\ 1,\ \ldots ,N/2\}, \tag{2}$$

where h_n denotes the time samples of a spectral widow, *i* is the index of spectral line, *m* is the index of the time slice and *l* is the number of time samples between two consecutive time slices in the spectrogram. In the resulting spectrogram, the time and frequency resolution compromise is fixed by the time length *N*. The *l* parameter fixes the time-slicing step of the spectrogram.

This paper explains how the phase spectrogram, using the phase of $S_{m,i}$, provides access to a source of information which completes that offered by the power spectrogram. The information in a phase spectrogram can take different forms. The easiest to understand intuitively is the phase variation of a sine wave compared to a reference sine wave, the latter being the same sine wave taken at a given time and not having changed its frequency since. On the other hand, in deriving this phase, we generate a frequency spectrogram that gives us a different perception of the instantaneous frequency.

PHASE UNWRAPPING

In this text, we use underscored notations to mean that the $\underline{\theta}$ phase is contained within the trigonometric circle. The underscored operator

$$\underline{*} = \mathrm{mod}_{2\pi}\{* + \pi\} - \pi \tag{3}$$

therefore removes the 2π multiple value in the operand. The phase value $\underline{\theta_{m,i}}$ comes from the trigonometric function atan2(*,*) applied to the result of the STFT such that

$$\underline{\theta_{m,i}} = \mathrm{atan}\,2\left(\mathrm{Re}\left(S_{m,i}\right), \mathrm{Im}\left(S_{m,i}\right)\right) \tag{4}$$

with $\underline{\theta_{m,i}} \in \left]-\pi,\pi\right]$. However, the latter phase value corresponds to the projection of the unwrapped phase in the trigonometric circle. The unwrapped phase value

$$\theta_{m,i} = \underline{\theta_{m,i}} + \vartheta_{m,i}\cdot 2\pi \quad \text{with } \vartheta \in \mathbb{Z}, \tag{5}$$

differs by ϑ rotations in the trigonometric circle; we know the position of the phase on the circle but not the number of rotations. Phase unwrapping amounts to finding this number, which is done progressively by tracing round the trigonometric circle

repetitively, usually starting from a chosen reference point.

Several publications deal with phase unwrapping on the frequency axis [7-12] but no author presents the phase unwrapping on the time axis in the time-frequency plane. However, whether it be the frequency or the time axis, phase unwrapping consists in selecting the shortest path on the trigonometric circle. Classically, the unwrapping can only be achieved if the phase does not vary by more than π radians between two successive time slices. In the proposed algorithm, the phase may vary by many π radians between two successive time slices.

The phase-unwrapping algorithm in time is recursive and usually starts with the first time slice. A simple form of this algorithm, starting with the first sample, consists in writing

$$\theta^*_{m,i} = \underline{\theta_{m,i}} + \vartheta_{m,i} \cdot 2\pi \quad \text{with } \vartheta_{m,i} \in \mathbb{Z}, \tag{6}$$

where ϑ_m corresponds to the number of rotations or turns completed in the trigonometric circle. The integer $\vartheta_{m,i}$ is established recursively such that

$$\vartheta_{m,i} = \begin{cases} \vartheta_{m-1,i} & \text{for } -\pi < \underline{\theta_{m,i}} - \underline{\theta_{m-1,i}} \le \pi \\ 1 + \vartheta_{m-1,i} & \text{for } \underline{\theta_{m,i}} - \underline{\theta_{m-1,i}} \le -\pi \\ \vartheta_{m-1,i} - 1 & \text{for } \pi < \underline{\theta_{m,i}} - \underline{\theta_{m-1,i}} \end{cases} \quad \text{and} \quad \vartheta_{1,i} = 0, \tag{7}$$

so that any phase shift with an amplitude exceeding π can be attributed to the fact that the boundary - π / π of the trigonometric circle has been crossed. If the phase sampling condition is respected, then $\theta^*_{m,i} = \theta_{m,i}$. For simplification, we write

$$\theta_{m,i} = \text{unwrap}\left(\underline{\theta_{m,i}}\right) \tag{8}$$

to express the unwrapping of the phase. The operator unwraps the phase without worrying about there being possibly *n* extra 2π radians between two consecutive time slices.

FREQUENCY SPECTROGRAM

The wrapped frequency spectrogram

$$f_{m,i}(P) \equiv \frac{f_s}{2\pi \cdot l \cdot P} \cdot \underline{P\left(\underline{\theta_{m,i}} - \underline{\theta_{m-1,i}}\right)} \tag{9}$$

is obtained from the phase difference between successive time slices of the STFT where $P \in \mathbb{Z}$ and f_s is the sampling rate. A mathematical demonstration has been developed and can be found in [13]. The gain *P* multiplies the sensitivity expressed as the fringes per Hz in such a way that

$$f_{m,i}(P) \in \left]-\frac{f_s}{2lP}, \frac{f_s}{2lP}\right] \tag{10}$$

defines the frequency axis scaling. All we need do is display the frequency on a scale of colors where the two extremes - $f_s/2lP$ and $f_s/2lP$ have the same color, in order to

watch the frequency develop without any break in the progression. The gain P is adjusted so that the progression can be monitored and we can easily count the fringes on the screen. The sensitivity f_s/lP is expressed in Hz/fringe.

We should emphasize that this definition of the frequency spectrogram depends largely on the equality $\underline{P\left(\theta_{m,i} - \theta_{m-1,i}\right)} = \underline{P\left(\theta_{m,i} - \theta_{m-1,i} + \vartheta 2\pi\right)}$ for integers ϑ and P. With an integer value gain, we amplify the phase difference between two time slices without any disturbance from an error in the estimation of a phase of "ϑ" turns in the trigonometric circle: we no longer need to know the number of rotations of the unwrapped phase value before applying the gain.

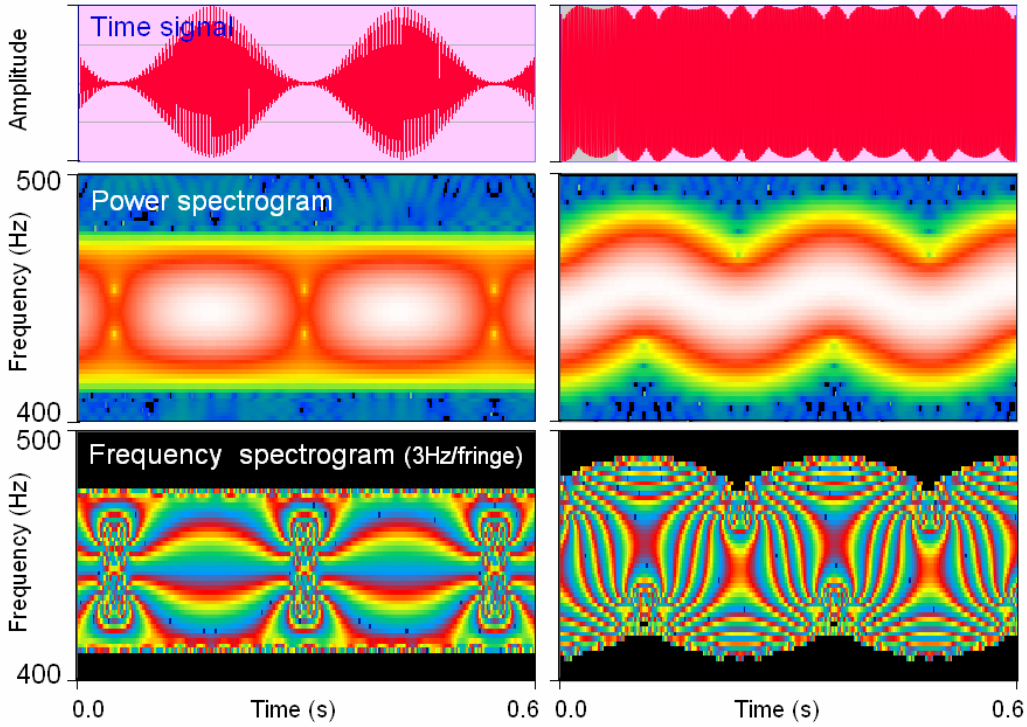

Figure 1 – Time series, power spectrogram and frequency spectrogram of an amplitude-modulated generated signal (left) and of a frequency-modulated generated signal (right).

Once an integer value gain has been applied, we can unwrap the phase. In fact, the unwrapped frequency spectrogram

$$f_{m,i}^{\mathrm{U}}\left(P, m_r\right) \equiv \frac{f_s}{2\pi \cdot lP}\left(\mathrm{unwrap}\left(P\left(\underline{\theta_{m,i}} - \underline{\theta_{m-1,i}}\right)\right) - \mathrm{unwrap}\left(P\left(\underline{\theta_{m_r,i}} - \underline{\theta_{m_r-1,i}}\right)\right)\right)$$

$$\text{for } m = 2, 3, 4, \ldots, M \qquad (11)$$

allows us to display the frequency relative to the reference slice m_r on a continuous scale. The frequency presents the same topological characteristic as the phase in the trigonometric circle, which means that it can be illustrated as superposed on a cyclic

scale (Eq. 9) or unwrapped on a conventional scale (Eq. 11).
The term $P\left(\underline{\theta_{m,i}} - \underline{\theta_{m-1,i}}\right)$ in Eqs.9 and 11 can be replaced by

$$\sum_{k=1}^{N_P} P_k \left(\underline{\theta_{m+k,i}} - \underline{\theta_{m+k-1,i}}\right) \tag{12}$$

for weighting the computation of the phase derivative. This smoothing distributes the gain P according to an approximately Gaussian distribution of smaller weight P_i so that

$$P = \sum_{k=1}^{N_P} P_k \tag{13}$$

with integers P_i. The advantage of the weighting is that we obtain smoothing with a Gaussian distribution whereas increasing the distance l between slices amounts to having a smoothing with a rectangular window where $P = P_i N_p$.

Figure 1 depicts the processing results of two numerically-generated cosines. Amplitude modulation shows a horizontal fringe pattern (Fig. 1 left). On the opposite, the modulation of phase or frequency generates a fringe pattern perpendicular to the path of the sine wave in the time-frequency plane (Fig. 1 right). Since the instantaneous frequency of a sine wave has no significance other than below the main lobe of the corresponding spectral component, only the result under the main lobe is displayed. In order to do this, we fill in the corresponding power spectrogram valleys in black to drown the secondary components with the lowest amplitudes. The height of the filling is adjusted manually by the user, depending on the amount of information to be underlined. For the amplitude modulated examples, a 4X spectral interpolation is required to be able to display smoothly the fringe pattern.

PHASE SPECTROGRAM

The phase difference is equal to

$$2\pi \cdot \frac{l \cdot P}{f_s} \cdot f_{m,i}^{\mathrm{U}}\left(P, m_r\right) + C \tag{14}$$

between two successive time slices where C is an unknown corresponding to the number of complete turns in the trigonometric circle between two successive slices of the STFT. The mean frequency of the component thus determines the magnitude of C. The information that C contains is of little use because the focus of our interest is the phase variations around the mean increment in the phase increase, not the slope of the phase increase due to the mean frequency of the component. Therefore, if we remove C from the computation, numerical integration of the type:

$$\Phi_{m,i}\left(P, m_r\right) = \begin{cases} 0, & m = 1 \\ 2\pi \cdot \dfrac{l}{f_s} \displaystyle\sum_{j=2}^{m} f_{j,i}^{\mathrm{U}}\left(P, m_r\right), & m = 2, 3, ..., M \end{cases} \tag{15}$$

yields an unwrapped-phase value starting from the first time slice. In (15), the phase calculation is referenced to both the first slice for calculating the phase and slice m_r for calculating the reference frequency. The latter frequency determines the phase constant to be removed between each slice so as to eliminate the constant term of the phase increase. The generalized phase spectrogram defined as

$$\theta^{\mathrm{G}}_{m,i}\left(P,m_r\right) \equiv \Phi_{m,i}\left(P,m_r\right) - \Phi_{m_r,i}\left(P,m_r\right) \tag{16}$$

allows us to refer both the phase calculation and the frequency calculation simultaneously to the m_r^{th} time slice. For a display with a succession of fringes, we use this presentation $\underline{\theta^{\mathrm{G}}_{m,i}\left(P,m_r\right)}$ but we could also write

$$\underline{\theta^{\mathrm{G}}_{m,i}} = \underline{\Phi_{m,i}\left(P,m_r\right) - \frac{m-1}{M-1}\Phi_{M-1,i}\left(P,m_r\right)} \tag{17}$$

if we want to impose a null phase value on the two extremities of the measurement as in the phase spectrogram illustrated in Fig. 2.

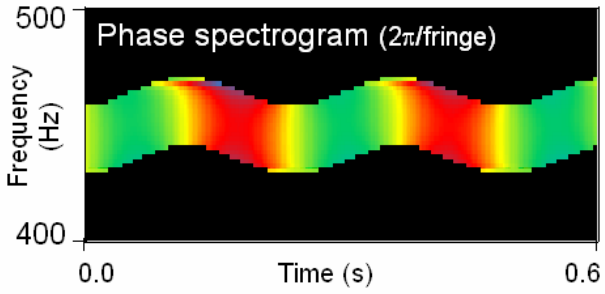

Figure 2 - Phase spectrogram of a sine wave with a phase modulation of ±π radians, with f_S=2 ks/s (N=128 samples, 2X spectral interpolation, l=5 and P=1) Note the π/2 radians delay between the frequency and phase. The power spectrogram is shown in Fig. 1, right.

If the distance l and the distribution P_i have an influence on the variance in the frequency spectrogram, they have none on the phase spectrogram [13]. In the latter case, the distance l affects the graphic definition on the time axis while the weight P restrains the phase to the interval] -π/P, π/P], superposing the distribution of phase values for no useful purpose. The weight P is therefore set at unity for calculating the phase spectrogram and the feature proposed in Eq.12 is not used. The numerical example in Fig. 2, the function $\cos\left(2\pi\cdot 200\text{Hz}\cdot t + \pi\cdot\cos\left(2\pi\cdot 2\text{Hz}\cdot t\right)\right)$, shows the presence of a uniform phase plateau across the width of the main lobe of the component. Also, as in the frequency spectrogram with a phase modulation, the phase spectrogram of a phase modulation shows perpendicular fringes in the path of the sine wave while an amplitude modulation shows fringes in the opposite direction on the phase spectrogram (not illustrated. See [13]).

APPLICATIONS TO MONITORING AND DIAGNOSTICS

A vibrating-string sensor is commonly used for concrete deformation measurements in bridges and dams. The string frequency is a linear function of the deformation. Some of these sensors comprise an excitation coil and a reading coil, both connected to an electronic conditioner. In the continuous-excitation operating mode, the coils and conditioner are connected in a closed-loop feedback. Figure 3 illustrates the sensitivity of the apparatus to an electromagnetic disturbance at power system frequency when the string was tested in our laboratory. The frequency spectrogram shows a 5-Hz peak-to-peak frequency ripple, which can be eliminated using a counting period multiple of 16.6 ms.

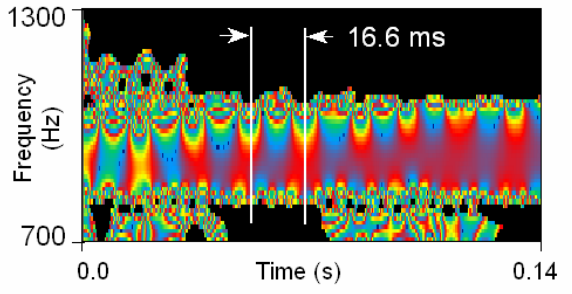

Figure 3 - Frequency spectrogram of a vibrating-string signal. The P value yields a 10-Hz/fringe sensitivity. The frequency modulation, at 16.6-ms pitch, is explained by an electronic disturbance coming from the 60-Hz system frequency.

The phase and frequency spectrograms are also good tools for revealing slight changes in the frequency of the free damping response of excited modes [14,15]. Figure 4 illustrates a result obtained for a metallic cantilever beam with a small crack in it. Soon after the mechanical impact, a short-time frequency drift appears. This drift corresponds to the transition between two vibration states: that where the displacement has enough amplitude to fully open the crack and that where the crack remains closed. On the phase spectrogram, the cursor sets the time reference slice m_r close after the impact end in order to shown six fringes, or cycles, in 250 ms: a 24-Hz frequency drift. Other case studies are available in [16].

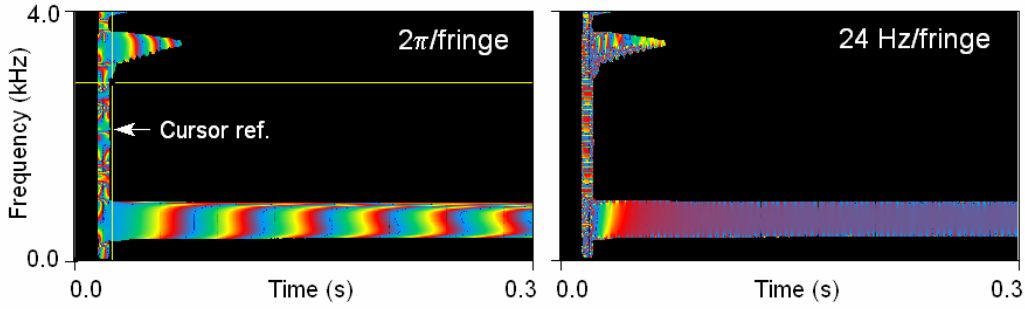

Figure 4 - Phase spectrogram (left) and frequency spectrogram (right) of the free response of a 6.2% surface ratio cracked beam excited by a 2kN mechanical impact. (fs=25.6 ks/s)

CONCLUSIONS

Phase spectrogram and frequency spectrograms make the information contained in the phase of the STFT useful. The phase information presented in the time-frequency plane can be applied for accurate diagnostic purposes. Fringe patterns can be seen allowing us to distinguish between weak frequency modulation and an amplitude modulation. The capacity to distinguish these modulations in the visual interpretation opens the way to new diagnostic approaches. The LabView™ code and runtime are available on request.

REFERENCES

[1] D. GABOR, "Theory of communication", *J. IEE*, **93**, No. 3, p. 429-457, 1946.

[2] J. VILLE, "Théorie et applications de la notion de signal analytique", *Cables & Transmission*, **2** A, No. 1, p. 61-74, 1948.

[3] L. COHEN, "Time-Frequency Distribution - A Review", *Proc. IEEE*, **77**, No. 7, p. 941-981, 1989.

[4] F.AUGER, P. FLANDRIN, "Improving the readability of time-frequency and time-scale representations by using the reassignment method", *IEEE Trans. on Signal Proc.*, **43**, No.5, p 1068-1089, 1995.

[5] K.KODERA, R. GENDRIN, C. DE VILLEDARY, "Analysis of Time-Varying Signals with Small *BT* Values", *IEEE Trans. ASSP*, **26**, No.1, p 64-76, 1978.

[6] P. FLANDRIN, "Time-Frequency and Time-Scale", *Spectrum Estimation and Modeling*, Fourth Annual ASSP Workshop on Published:1988, p 77-80, 1988.

[7] A. V. OPPENHEIM, R. W. SCHAFER, *Digital Signal Processing*, Prentice-Hall Inc., N. Jersey, 1975.

[8] W. B. HERSHEY, J. M. KIM, "Impulse response applications to nondestructive testing", *International Advances in Nondestructive testing*, **15**, p.289-311, 1990.

[9] J.M. TRIBOLET, "A new phase unwrapping algorithm", *IEEE Transaction on Acoustics, Speech and Signal Proccessing*, **25**, No. 2, avril 1977.

[10] B. BHANU, J.H. MCCLELLAN, "On the computation of the complex cepstrum", *IEEE Transaction on Acoustics, Speech and Signal Proccessing*, **28**, p. 583-585, 1980.

[11] R. MCGOWAN, R. KUC, "A direct relation between a signal time series and its unwrapped phase", *IEEE Transaction on Acoustics, Speech and Signal Proccessing*, **30**, p. 719-726, 1982.

[12] H. NASHI, "Phase unwrapping of digital signals", *IEEE Transaction on Acoustics, Speech and Signal Proccessing*, **37**, No. 11, p. 1693-1702, 1989.

[13] F.LÉONARD, "Spectrogramme de phase et spectrogramme de fréquence", *Revue du Traitement du Signal*, **17**, No. 4, p. 269-286, avril 2001.

[14] F.LÉONARD, J. LANTEIGNE, S. LALONDE, AND Y.TURCOTTE, " Vibration behavior of a cracked cantilever beam", *18th Int. Modal Analysis Conf.*, San Antonio, Texas, février 2000.

[15] F.LÉONARD, J. LANTEIGNE, S. LALONDE, AND Y.TURCOTTE, "Vibration behavior of a cracked cantilever beam", *Mechanical Systems and Signal Processing*. **15**, No. 3, p. 259-548, 2001.

[16] F.LÉONARD, , "Phase spectrogram and frequency spectrogram as new diagnostic tools", *Mechanical Systems and Signal Processing*. Available online, 2005.